

Determination of the confocal volume of a Raman microscope for probing for single-molecule SERS applications.

Flávia Campos Marques*(flavia@ice.ufjf.br) and Gustavo Fernandes Souza Andrade (gustavo.andrade@ufjf.br).

Departamento de Química, Universidade Federal de Juiz de Fora, CEP 36036-900, Juiz de Fora, MG, Brasil.

Article history: Received: May 10, 2023; revised: September 21, 2023; accepted: November 14, 2023;
Available online; DOI:

Abstract

In Raman spectroscopy, the confocal volume refers to the sample region from which scattered photons are collected by a confocal Raman spectrometer, defined by the cone-shaped light beam generated by the objective lens of the microscope in the confocal configuration. The confocal volume is characterized by the confocal height and confocal area, which determine the range of heights and lateral positions, respectively, from which the spectrometer effectively collects the scattered photons. In the present study, the confocal height and area were calculated for different configurations of a confocal Raman spectrometer to obtain the confocal volume using a Si wafer sample. Understanding the confocal volume is essential for optimizing Raman microscopy experiments and for estimating the number of molecules that generate surface-enhanced Raman spectroscopy spectra in a single-molecule regime.

Keywords: Confocal volume. Confocal height. Confocal area. Raman spectrometer. SERS.

1. Introduction

Raman spectroscopy is a technique that allows the detection and identification of chemical species and has been covering several fields, such as physics, chemistry, the pharmaceutical industry, art, and much more [1–7]. However, the weak signals caused by the low cross section for the Raman effect limit the use of Raman spectroscopy for some systems, such as analysis in dilute solutions. Surface-enhanced Raman scattering spectroscopy (SERS) is a strategy used to circumvent this limitation [8–10]. SERS results in increased Raman intensities of molecules attached to plasmonic Au, Ag, and Cu nanoparticles (NPs) [11,12]. SERS enhancements can reach up to eight orders of magnitude or even higher values in regions of strongly confined electromagnetic fields, known as “hot spots” [13–15]. The

presence of “hot spots” increases SERS efficiency, which allows the detection of a single molecule (SM) [16–19]. SM-SERS allows obtaining information about the molecular structure of a molecule at very low concentrations, on the order of nanomolar. In this context, it is necessary to determine the actual number of molecules adsorbed in the confocal volume to obtain the SM-SERS signal. Once the correct number of molecules is known, the concentration of the molecules in the SM-SERS signal can be calculated. Therefore, reaching the detection limit of a single molecule for SERS depends closely on the confocal volume of the Raman microscope used for probing.

The confocal volume of a Raman spectrometer is the “in-focus” volume within the sample. It is determined by the region of space in which the focused light forms a volume, which is limited by specific geometric conditions, such as the spot size in focus and depth of focus, which vary according to the specific experimental conditions (*e.g.*, wavelength, objective, and confocal aperture) [4]. The principle of confocal Raman spectroscopy is related to the telescope principle, in which an objective lens focuses the light source and a second lens, ocular, is mounted at the proper position relative to the first focus, collimating light to an observer, which results in an alteration of the spot area and depth of focus, allowing focusing laser lines on tight spots. The initial development of laser confocal microscopy by Egger and Davidovits [20,21] was intended to improve the lateral and depth resolutions of fluorescence microscopy for *in vivo* fluorescence measurements. The confocal aperture plays a relevant role in the improved lateral resolution before the detector in the above-cited optical confocal setups; the slit removes most of the spectroscopic signal, leaving only light close to the focal plane of the objective to reach the detector. It was also developed to perform three-dimensional images by moving in the height (Z-axis) direction. A confocal microscope scheme is presented in Fig. 1, where one may notice that the expanded laser beam is focused by the objective on the sample in a tiny spot in the focal plane, typically with an area in the micrometer-square range. The light emitted or scattered by the sample will present different paths in the lens system depending on whether it comes from the focal plane or other regions of the sample. The different optical paths limit the amount of light directed to the detector by the confocal slit, which preferentially transmits light from heights close to the focal plane. That limits the detection of light to a small volume close to the center of the laser spot and to the focal plane, which may be referred to as ‘confocal volume’ above.

Figure 1: Schematic depicting the optics of a confocal microscope, demonstrating the incorporation of a "confocal aperture" which confines the sampling depth; a) in the focal plane at $Z=0$ e b) Out-of-focus within a transparent sample.

Confocal Raman spectrometers present multiple approaches to reach the confocal selection of light. To the best of our knowledge, three different approaches are commercially available: one approach is based on the traditional use of adjustable slits that select the in-focus light, as described above; the second approach uses optical fibers to both generate beam expansion and works as a slit in the collection of light; and the third approach is based on the selection of the in-focus light based on the selection of the area in the multichannel detector (in all three cases, the detectors are usually charge-coupled displays, CCD). The first two approaches rely on adjustable apertures that impair part of the light scattered out of focus to reach the detector. The entire detector area can detect any light passing through the apertures. The third approach uses, instead of apertures, an electronic selection of the detector area that receives the Raman signal; the selection of the detector area results in the loss of most of the Raman intensity but selects the scattered light that is in focus. In the present study, the Raman spectrometer uses the second approach, which uses optical fibers as beam expanders and sends it to the spectrometer light that passes through adjustable apertures.

Raman spectroscopy has been developed into confocal spectrometers for at least three decades, allowing for the study of many samples [22]. SERS spectroscopy may allow for the determination of molecules found in the confocal volume of a colloidal suspension [23]. A

procedure to resolve this volume may enable determination of the maximum concentration that would result in an average of one molecule per confocal volume, resulting in a single-molecule SERS regime. Thus, it is necessary to determine the confocal volume of the Raman spectrometer used to detect a single molecule using SERS. However, to determine the confocal volume, two relevant quantities depend on the wavelength used: the area illuminated by the laser spot, and the height of the light cone.

In this work, we present in detail the determination of the confocal volume of a Raman spectrometer and then calculate the specific sample concentration for detecting a single molecule by SERS.

2. Experimental

2.1 Equipment measurement.

Raman spectra were obtained using a dispersive Raman spectrometer Bruker, model Senterra. The excitation radiation was the laser line at $\lambda_0=632.8$ nm with an exit power of 20 mW from a built-in HeNe laser or $\lambda_0=785$ nm with an exit power of 100 mW from a built-in solid-state laser. Spectral data were collected using a $50\times$ ULWD magnification objective lens (NA=0.51), (25×1000) μm^2 or (50×1000) μm^2 confocal aperture, and a spectral resolution of $3\text{-}5$ cm^{-1} .

3. Results and Discussion

The confocal volume refers to the shape of the light beam (cone-shaped) generated by the objective lens of the Raman microscope in the confocal configuration [24]. Fig. 2 shows the waist profile of the white light beam (reference light of the Raman spectrometer) in an aqueous suspension of Ag nanoparticles, which was used to observe the scattered light. In a regular spectrometer, all molecules present within this illuminated volume could contribute to the Raman and SERS signals detected by the spectrometer. However, in a confocal Raman setup, the collection of these scattered photons varies with depth relative to the focus (height difference around the focal plane) in the $+Z$ and $-Z$ -interval directions, as illustrated in Fig. 3. In the focal plane, at $Z = 0$, the intensity of the signal collected is maximum, and the variation with height is significant, which shows that only the light scattered in a specific range of heights close to the focal plane can be effectively measured by the spectrometer, defining the confocal height of the equipment.



Figure 2: Form of the white-light focus formed by the objective lens of the Raman microscope using a sample of Ag nanoparticles.

The confocal volume was characterized by the area illuminated by the laser spot (confocal area (A)) and the height of the cone of light that was effectively sampled when passing through the slit of the equipment (confocal height (H)) [23,25]. The volume close to the $Z=0$ focal plane was calculated as that of a cylinder (see Figure 2). A standard silicon sample was used to determine the confocal area and height, as shown in Fig. 3.

The confocal height was determined by maintaining a fixed position in the XY plane and varying the height along the axial axis around the focal plane $Z=0$, resulting in a confocal height given by height H in Fig. 2 (b). The integrated intensity of the most intense silicon band at 521.5 cm^{-1} was recorded by moving $+200 \text{ }\mu\text{m}$ upward and $-200 \text{ }\mu\text{m}$ downwards relative to the focal plane at $Z=0$ and acquiring Raman spectra every $2 \text{ }\mu\text{m}$.

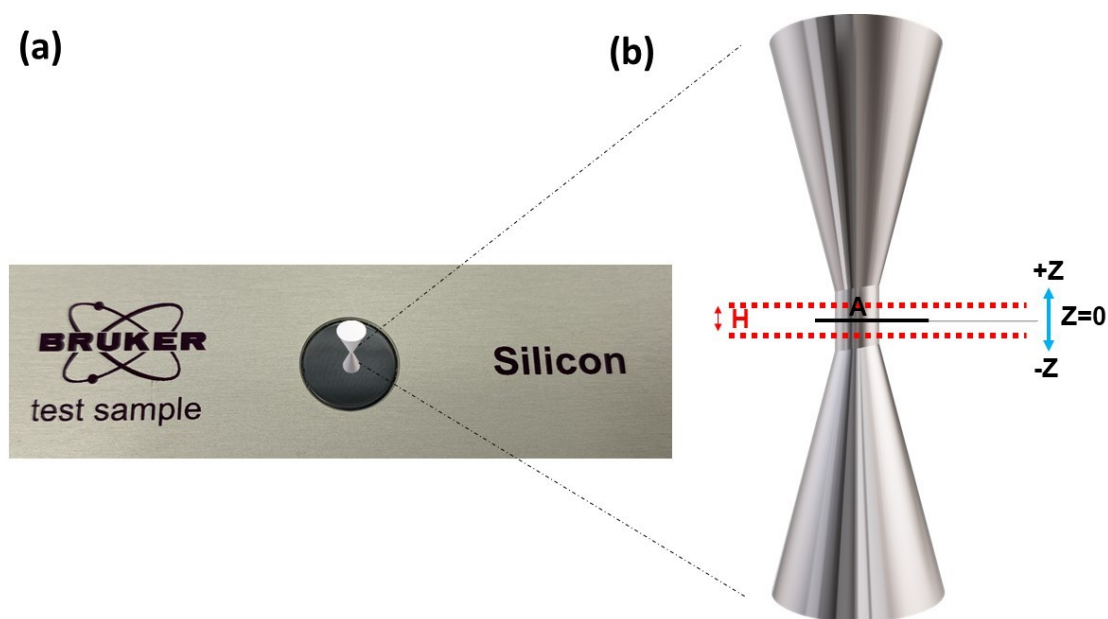


Figure 3: (a) Illustration of confocal volume in standard silicon sample. (b) In the focal plane at $Z=0$, A , the confocal area was measured, represented by a black line, where the two dashed red lines define the height limits, and their separation gives H , the confocal height, on the axial axis ($+Z$, $-Z$).

Fig.4 shows the variation of the integrated intensity of the silicon Raman band as a function of the axial shift using $\lambda_0=632.8$ nm with a laser power of 20 mW and confocal aperture of the spectrometer $50 \times 1000 \mu\text{m}$. Note that, at $Z=0$, the integrated intensity is at its maximum. Furthermore, it was observed that there was an abrupt decrease in the Raman signal about the ideally focused plane on both sides. It can be observed that the contribution of photons scattered in the standard silicon sample above $|Z| > 75 \mu\text{m}$ is negligible.

The confocal height was defined by an ultrathin effective layer H (Fig. 4), from which the entire spot laser signal was received. The confocal height was obtained using Equation 1 [23].

$$H = \frac{\int_{-200 \mu\text{m}}^{+200 \mu\text{m}} I(z) dz}{I_{\text{máx}}} \quad (1)$$

Where the numerator $\int_{-200\mu\text{m}}^{+200\mu\text{m}} I(z) dz$ is obtained by integrating the area under the curve $I(z)dz$ and $I_{\text{máx}}$ is the intensity of the band when $Z=0$. Measurements were performed in triplicate to minimize errors. In the present study, based on the confocal depth profile in Fig. 4, H could be calculated to be $(23.8 \pm 0.3) \mu\text{m}$. The value of H is $\pm Z$. Therefore, the total effective signal comes from the axial shifting of $11.9 \mu\text{m}$ above and below the focal plane $Z=0$.

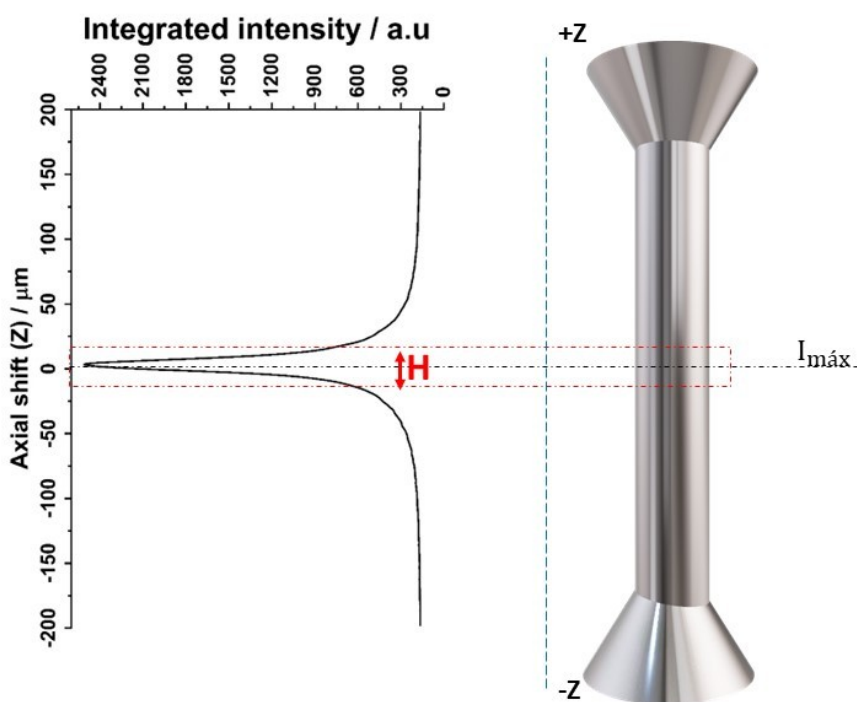


Figure 4: The integrated intensity of the most intense silicon band at 521.5 cm^{-1} was recorded by moving the motor stage $+200 \mu\text{m}$ up and $-200 \mu\text{m}$ down relative to the focal plane at $Z=0$ every $2 \mu\text{m}$.

The confocal area was determined by keeping the height fixed and shifting laterally along the x -axis through a linear scan that encompasses the abrupt interface of the standard silicon sample in the focal plane with a region that has no Si, as illustrated in the inset of Fig. 5 (b). The mapping covered a distance of $87.5 \mu\text{m}$, and the Raman spectrum was recorded every $0.437 \mu\text{m}$. It can be seen in Fig. 5 (a) the set of spectra obtained from the Raman mapping as a function of the lateral shift. Note that the laser intensity is close to zero outside the

standard silicon sample and is maximal at the focal plane within the region containing the standard silicon sample. The dependence of Raman intensity on the lateral shift is shown in Fig. 5 (b). At the interface between the silicon sample and the region without the silicon sample, there was an increase in the Raman intensity (approximately at $Z=100 \mu\text{m}$), which may be explained by the laser diffraction close to the interface of the Si sample. The sample was not entirely perpendicular to laser incidence at the interface. Outside this interface, the intensity value was relatively constant because it did not suffer from diffraction effects.

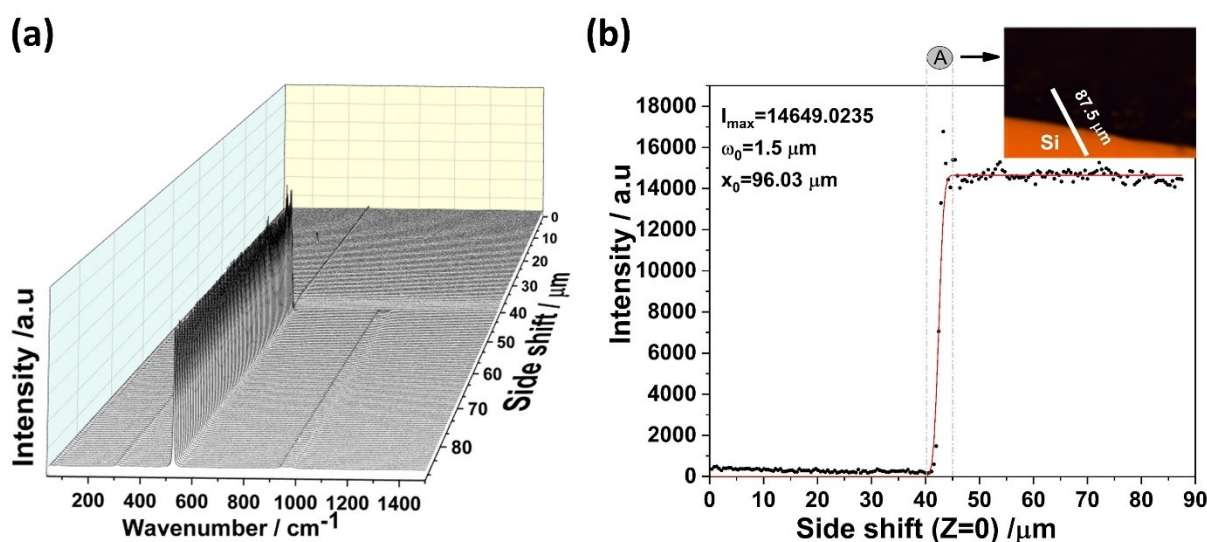


Figure 5: (a) Raman mapping obtained by a lateral shift of the Raman spectra of the Si standard sample and (b) Intensity profile of the Raman band at 521.5 cm^{-1} of the standard silicon sample as a function of the lateral shift. The inset shows a zoom of the lateral mapping in the standard silicon, encompassing a distance of $87.5 \mu\text{m}$.

The Raman intensity dependence along the x-axis can be described by Equation 2 [4,25]:

$$I(X) = \frac{I_{\text{máx}}}{2} \times \left(1 - \text{erf} \left(\frac{\sqrt{2} \times (X_0 - X)}{\omega_0} \right) \right) \quad (2)$$

Where $I(X)$ is the signal intensity on the x-axis, $I_{\text{máx}}$ is the maximum signal intensity, erf is the error function, x_0 is the position where 50% of the laser spot area is focused on the sample, and ω_0 is the confocal waist width. By adjusting Equation 2 in Fig. 5 (b), the parameter ω_0 could be extracted. Thus, the ω_0 value is $(1.6 \pm 0.1) \mu\text{m}$ for $\lambda_0 = 632.8 \text{ nm}$.

The area illuminated by the laser refers to the calculation of the area of the circular base of a cylinder, as given by Equation 3 [25].

$$A = \frac{P_0}{I_0} = \frac{\omega_0^2 \times \pi}{2} \quad (3)$$

Where P_0 is the incident power and I_0 is the intensity at the center of the focal plane. For the experimental setup, the excitation profile with waist $\omega_0 = 1.6 \mu\text{m}$ corresponds to a confocal area $A = 4.02 \mu\text{m}^2$. The effective scattering confocal volume can be calculated using Equation 4. From Equation 4 and the data presented above, we obtained an effective scattering confocal volume of $V = 9.57 \times 10^{-14} \text{L}$.

$$V = H \times A \quad (4)$$

The confocal volume depends on the configurations of the spectrometer. The concentration values were obtained by calculating the concentration of one molecule per volume in the confocal configuration determined using the methodology. Thus, the confocal volume was obtained by varying the confocal aperture and incident radiation. The characteristic concentration for single-molecule detection by SERS was determined through the confocal volume, and they are listed in Tab.1 and Tab. 2.

Table 1: Values of H, A, and concentrations in the single-molecule regime determined by the confocal volume for the laser line at 632.8 nm using 50×1000 μm and 25×1000 μm confocal apertures.

Laser line		632.8 nm		
<i>Confocal apertures (μm)</i>	A (μm ²)	H (μm)	Concentrations in the single molecule regime (mol L ⁻¹)	
50×1000	4.02	23.80	1.59×10 ⁻⁹	
25×1000	1.45	18.08	4.35×10 ⁻¹⁰	

Table 2: Values of H, A, and concentrations in the single-molecule regime determined by confocal volume for the laser line at 785 nm using the 50×1000 μm and 25×1000 μm confocal apertures.

Laser line		785 nm		
Confocal apertures (μm)	A (μm^2)	H (μm)	Concentrations in the single molecule regime (mol L^{-1})	
50×1000	5.26	31.25	2.72×10 ⁻¹¹	
25×1000	4.50	31.64	2.36×10 ⁻¹¹	

4. Conclusions

The assessment of the confocal profile of the Raman spectrometer yielded valuable insights, allowing us to extract essential parameters such as the area, height, and probed confocal volume of the laser. The concentrations used for detecting a single molecule by SERS were estimated using different spectrometer configurations. Specifically, for the 632.8 nm laser line, employing the 50×1000 μm confocal aperture led to values of 4.02 μm^2 (area), 23.80 μm (height), and 1.59×10⁻⁹ mol L⁻¹ (concentration in the SM regime). Correspondingly, the 25×1000 μm confocal aperture exhibited values of 1.45 μm^2 , 18.08 μm , and 4.35×10⁻¹⁰ mol L⁻¹, respectively. For laser lines at 785 nm, the 25×1000 μm confocal aperture revealed values of 5.26 μm^2 , 31.25 μm , and 2.72×10⁻¹¹ mol L⁻¹, while the 25×1000 μm confocal aperture was 4.50 μm^2 , 31.64 μm , and 2.36×10⁻¹¹ mol L⁻¹, respectively.

Confocal profiling analysis remains pivotal for establishing optimal conditions for the detection of single molecules via SERS. However, it is important to emphasize the significant dependence of Raman confocality on the specific configuration of the instrument. The values reported in this study are intrinsically linked to the intrinsic characteristics of the configuration used for the Raman spectrometer, such as wavelength, confocal aperture, beam geometry, and objective. Thus, the reported values should be interpreted and used with extreme caution by other Raman users while carefully considering the nuances of the experimental setup.

Acknowledgments

The authors thank CNPq, FAPEMIG, CAPES (financing code 001), and FINEP for financial support. FCM thanks CAPES for a fellowship.

References and Notes

- [1] K. Rebrosova, O. Samek, M. Kizovsky, S. Bernatova, V. Hola, F. Ruzicka, Raman Spectroscopy—A Novel Method for Identification and Characterization of Microbes on a Single-Cell Level in Clinical Settings, *Front Cell Infect Microbiol.* 12 (2022). <https://doi.org/10.3389/fcimb.2022.866463>.
- [2] J.-B. Wu, M.-L. Lin, X. Cong, H.-N. Liu, P.-H. Tan, Raman spectroscopy of graphene-based materials and its applications in related devices, *Chem Soc Rev.* 47 (2018) 1822–1873. <https://doi.org/10.1039/C6CS00915H>.
- [3] D.W. Shipp, F. Sinjab, I. Notingher, Raman spectroscopy: techniques and applications in the life sciences, *Adv Opt Photonics.* 9 (2017) 315. <https://doi.org/10.1364/AOP.9.000315>.
- [4] A. Sacco, C. Portesi, A.M. Giovannozzi, A.M. Rossi, Graphene edge method for three-dimensional probing of Raman microscopes focal volumes, *Journal of Raman Spectroscopy.* 52 (2021) 1671–1684. <https://doi.org/10.1002/jrs.6187>.
- [5] G.M. do Nascimento, V.R.L. Constantino, R. Landers, M.L.A. Temperini, Aniline polymerization into montmorillonite clay: A spectroscopic investigation of the intercalated conducting polymer, *Macromolecules.* 37 (2004) 9373–9385. <https://doi.org/10.1021/ma049054>.
- [6] G. Barzan, A. Sacco, L. Mandrile, A.M. Giovannozzi, C. Portesi, A.M. Rossi, Hyperspectral Chemical Imaging of Single Bacterial Cell Structure by Raman Spectroscopy and Machine Learning, *Applied Sciences.* 11 (2021) 3409. <https://doi.org/10.3390/app11083409>.
- [7] R.M. Romano, R. Stephani, L.F. Cappa de Oliveira, C.O. Della Védova, The Colour of the Argentinean Flag, *ChemistrySelect.* 2 (2017) 2235–2240. <https://doi.org/10.1002/slct.201700284>.
- [8] M. Fan, G.F.S. Andrade, A.G. Brolo, A review on recent advances in the applications of surface-enhanced Raman scattering in analytical chemistry, *Anal Chim Acta.* 1097 (2020) 1–29. <https://doi.org/10.1016/j.aca.2019.11.049>.
- [9] M. Fan, G.F.S. Andrade, A.G. Brolo, A review on the fabrication of substrates for surface enhanced Raman spectroscopy and their applications in analytical chemistry, *Anal Chim Acta.* 693 (2011) 7–25. <https://doi.org/10.1016/j.aca.2011.03.002>.
- [10] G.F.S. Andrade, Q. Min, R. Gordon, A.G. Brolo, Surface-Enhanced Resonance Raman Scattering on Gold Concentric Rings: Polarization Dependence and Intensity Fluctuations, *The Journal of Physical Chemistry C.* 116 (2012) 2672–2676. <https://doi.org/10.1021/jp2087362>.

- [11] F.Y.H. Kutsanedzie, A.A. Agyekum, V. Annaram, Q. Chen, Signal-enhanced SERS-sensors of CAR-PLS and GA-PLS coupled AgNPs for ochratoxin A and aflatoxin B1 detection, *Food Chem.* 315 (2020) 126231. <https://doi.org/10.1016/j.foodchem.2020.126231>.
- [12] F.C. Marques, G.P. Oliveira, R.A.R. Teixeira, R.M.S. Justo, T.B.V. Neves, G.F.S. Andrade, Characterization of 11-mercaptoundecanoic and 3-mercaptopropionic acids adsorbed on silver by surface-enhanced Raman scattering, *Vib Spectrosc.* 98 (2018) 139–144. <https://doi.org/10.1016/J.VIBSPEC.2018.07.015>.
- [13] H. Wei, H. Xu, Hot spots in different metal nanostructures for plasmon-enhanced Raman spectroscopy, *Nanoscale.* 5 (2013) 10794–10805. <https://doi.org/10.1039/c3nr02924g>.
- [14] A. Lee, G.F.S. Andrade, A. Ahmed, M.L. Souza, N. Coombs, E. Tumarkin, K. Liu, R. Gordon, A.G. Brolo, E. Kumacheva, Probing Dynamic Generation of Hot-Spots in Self-Assembled Chains of Gold Nanorods by Surface-Enhanced Raman Scattering, *J Am Chem Soc.* 133 (2011) 7563–7570. <https://doi.org/10.1021/ja2015179>.
- [15] E.C. Le Ru, P.G. Etchegoin, M. Meyer, Enhancement factor distribution around a single surface-enhanced Raman scattering hot spot and its relation to single molecule detection, *Journal of Chemical Physics.* 125 (2006) 1–14. <https://doi.org/10.1063/1.2390694>.
- [16] F.C. Marques, R.S. Alves, D.P. dos Santos, G.F.S. Andrade, Surface-enhanced Raman spectroscopy of one and a few molecules of acid 4-mercaptobenzoic in AgNP enabled by hot spots generated by hydrogen bonding, *Physical Chemistry Chemical Physics.* 24 (2022) 27449–27458. <https://doi.org/10.1039/D2CP03375E>.
- [17] E.J. Blackie, E.C. le Ru, P.G. Etchegoin, Single-Molecule Surface-Enhanced Raman Spectroscopy of Nonresonant Molecules, *J Am Chem Soc.* 131 (2009) 14466–14472. <https://doi.org/10.1021/ja905319w>.
- [18] S.S.R. Spectroscopy, Single-Molecule Surface-Enhanced Raman Spectroscopy, (2022) 1–16. Surface-Enhanced Raman Scattering, *Acc Chem Res.* 52 (2019) 456–464. <https://doi.org/10.1021/acs.accounts.8b00563>.
- [20] P. DAVIDOVITS, M.D. EGGER, Scanning Laser Microscope, *Nature.* 223 (1969) 831–831. <https://doi.org/10.1038/223831a0>.
- [21] P. Davidovits, M.D. Egger, Scanning Laser Microscope for Biological Investigations, *Appl Opt.* 10 (1971) 1615. <https://doi.org/10.1364/AO.10.001615>.
- [22] M. Fries, A. Steele, Raman Spectroscopy and Confocal Raman Imaging in Mineralogy and Petrography, in: T. Dieing, O. Hollricher, J. Toporski (Eds.), *Confocal Raman Microscopy*,

- Springer Berlin Heidelberg, Berlin, Heidelberg, 2011: pp. 111–135.
<https://doi.org/10.1007/978-3-642-12522-5>.
- [23] W.B. Cai, B. Ren, X.Q. Li, C.X. She, F.M. Liu, X.W. Cai, Z.Q. Tian, Investigation of surface-enhanced Raman scattering from platinum electrodes using a confocal Raman microscope: dependence of surface roughening pretreatment, *Surf Sci.* 406 (1998) 9–22.
[https://doi.org/10.1016/S0039-6028\(97\)01030-3](https://doi.org/10.1016/S0039-6028(97)01030-3).
- [24] A.H.J. Kim, H. Suleiman, A.S. Shaw, New approaches in renal microscopy, *Curr Opin Nephrol Hypertens.* 25 (2016) 159–167. <https://doi.org/10.1097/MNH.0000000000000220>.
- [25] E.C. Le Ru, E. Blackie, M. Meyer, P.G. Etchegoint, Surface enhanced raman scattering enhancement factors: A comprehensive study, *Journal of Physical Chemistry C.* 111 (2007) 13794–13803. <https://doi.org/10.1021/jp0687908>.